Superlattices and Microstructures 91 (2016) 331–344

Contents lists available at ScienceDirect

Superlattices and Microstructures

journal homepage: www.elsevier.com/locate/superlattices

Influence of out-of-plane defects on vibration analysis of graphene: Molecular Dynamics and Non-local Elasticity approaches

S.K. Jalali [a, *], E. Jomehzadeh [b], N.M. Pugno [c, d, e]

[a] Department of Mechanical Engineering, Kermanshah University of Technology, Kermanshah, Iran
[b] Department of Mechanical Engineering, Graduate University of Advanced Technology, 7631133131, Kerman, Iran
[c] Laboratory of Bio-Inspired & Graphene Nanomechanics, Department of Civil, Environmental and Mechanical Engineering, Università di Trento, Via Mesiano, 77, I-38123, Trento, Italy
[d] Center for Materials and Microsystems, Fondazione Bruno Kessler, Via Sommarive 18, 38123, Povo, Trento, Italy
[e] School of Engineering & Materials Science, Queen Mary University of London, Mile End Road, London E1 4NS, UK

ARTICLE INFO

Article history:
Received 16 October 2015
Received in revised form 20 December 2015
Accepted 20 January 2016
Available online 28 January 2016

Keywords:
Defective graphene
Molecular dynamics
Nonlocal elasticity
Vibration

ABSTRACT

Out-of-plane defects may exist in graphene inevitably or purposely. The present study aims at investigating the influence of out-of-plane defects on vibrational analysis of single layered graphene sheets (SLGSs) implementing both nonlocal elasticity and molecular dynamics (MD) simulations. In nonlocal elasticity analysis, the defect is considered as an initial curvature which is modeled by an analytical function having controllable parameters for the amplitude, extension, and location. In molecular dynamics analysis, defects are simulated by inserting inverse Stone–Wales defects in the perfect structure of SLGSs. Both nonlocal continuum and MD simulation results reveal that the defects increase the vibrational frequency. It is shown that classical elasticity overestimates frequencies with a considerable error while the nonlocal plate model can fit MD results by implementing a proper small scale parameter.

1. Introduction

Graphene, the latest discovered carbon nanostructure, having its especial two dimensional (2D) geometry, has rapidly outpaced other well-known carbon nanostructures, i.e. fullerenes (zero-dimensional) and carbon nanotubes (one-dimensional), in most fields of researches due to its exclusive mechanical, thermal, and electronic properties [1]. Recently, investigations on graphene are extensively performed in various domains like fabrication methods of graphene sheets (GSs) [2], its wide applications in life, healthcare and technology [3], determination of its unique physical, mechanical and electrical properties [4] and developing theories and mathematical models for simulating GSs [5].

Ideally, carbon atoms of graphene are arranged on a flat plane inside a perfect hexagonal lattice. However, experimental observations [6] as well as atomistic simulations [7] verified the existence of inevitable defects in graphene structure during its fabrication process, which alters its perfect two dimensional hexagonal lattice and significantly affects its physical, mechanical, and electrical properties [8]. The defects in graphene can be categorized based on the genesis mechanisms: removing carbon atoms (vacancies), adding carbon atoms or other impurities (adatoms), and rearrangement of existing

* Corresponding author.
E-mail addresses: kjalali@kut.ac.ir, seyed.kamal.jalali@gmail.com (S.K. Jalali).

http://dx.doi.org/10.1016/j.spmi.2016.01.023
0749-6036/

carbon atoms (different ring sizes like Stone–Wales defects made by rotating a carbon bond). In the past years, vacancies and Stone–Wales defects and their influence on properties of GSs were comprehensively studied [9,10]. These defects are considered to alter the graphene lattice in its plane and therefore GSs remain 2D. Nevertheless, it is shown by both experimental observations [11] and atomistic simulations [12] that in the presence of specified types of defects graphene reshapes to a three dimensional (3D) state to minimize its energy. One of the most common out of plane defects is observed near the grain boundary regions of GSs fabricated by chemical vapor deposition (CVD). Liu et al. [13,14] carried out a series of hybrid molecular dynamics simulations to study the structures, energies, and structural transformations of grain boundaries of graphene and calculated the arrangement of pentagon/heptagon defects and associated out-of-plane deformations up to almost 3 Å in grain boundaries, depending on the chirality and tilt angles of grains. Yazyev and Louie [15], introduced a general approach for constructing the dislocations in graphene grain boundaries using *ab initio* calculations and investigated strong tendency toward out-of-plane deformation. They showed that defects in grain boundaries have important effects on physical properties of graphene and mentioned that these effects may be used for engineering graphene-based nano-materials and functional devices.

Against inevitable out-of-plane defects like grain boundary defects, recent studies suggest manipulating progresses to control position and type of defects using scanning tunneling microscopy (STM), atomic force microscopy (AFM), and ion or electron irradiation to create engineered desirable defects that modify properties of graphene [16–20]. Accordingly, some researchers have been motivated to design desired shapes and tune properties of graphene by manipulating out-of-plane defects. Lusk and Carr [21,22] proposed a method for engineering defects in graphene by introducing defect domains and presented a set of stable defects. Using density functional theory (DFT) they showed that some of these defects rise up out of the sheet about several angstroms. The possibility of controlling the shape of graphene using defects based on both continuum and atomistic simulations was investigated by Zhang et al. [23]. They adopted a generalized von Karman equation for a flexible solid membrane to describe graphene wrinkling induced by a prescribed distribution of topological defects and revealed that the proposed continuum model was capable of accurately predicting the atomic scale wrinkles near defects. Also, it was shown that under specific defect distributions it is possible to generate controlled large scale graphene configurations. The influence of out-of-plane curvature of a monolayer graphene on its bending behavior was investigated by Jomehzadeh et al. [24]. It was found that the proper configuration of initial curvature suggests the possibility of a smart stiffening tuning.

Recently, GSs have offered great promise for application in nano-electro-mechanical systems, especially as Gigahertz oscillators, resonant mass sensors, and ultra-high frequency nanoresonators [25,26]. Consequently, the vibrational characteristics of GSs have been extensively studied considering both continuum [27–32] and molecular [33,34] approaches. From a continuum perspective, a GS due to its planar geometry is assumed as a nanoplate and the associated well-known plate theories are employed to predict its response against mechanical loadings. To consider the discreteness of GSs, classical continuum elasticity is usually modified by adding a small scale parameter. Reviewing the literature reveals that the nonlocal elasticity of Eringen [35] has been widely employed to consider size effects in carbon nanostructures and its results are in a good agreement with those obtained by molecular approaches [36].

Notifying the possibility of generating controllable defects in graphene sheets, one may be motivated to use continuum plate for modeling GSs with out-of-plane defects. Historically, out-of-plane defects of plates have been an attractive issue among researchers in the field known as “plates with initial geometric imperfections”. These imperfections refer to permanent small deviations from the perfect flat shape of plates. It is reported that these initial imperfections can significantly affect response of plates to bending, vibration, and buckling loading situations [37,38]. Therefore, it may also be tempting to extend the idea to nanoplates and take into account inevitable or engineered out-of-plane defects of GSs as initial geometric imperfections.

According to the aforementioned review, out-of-plane defects may exist in GSs inevitably or purposely. On the other hand, potential application of GSs as resonators has been widely addressed and consequently, investigating the influence of defects on vibrational behavior of GSs may have significant outcomes for designing more efficient graphene-based resonators and sensors. Therefore, this work aims to study the influence of defects on the vibration behavior of single layered graphene sheets (SLGSs) via both nonlocal continuum elasticity and molecular dynamics approaches. At first, a SLGS is considered as a nanoplate with an initial geometric imperfection then a parametric study is carried out to explore the effects of shape and amplitude of initial imperfection, nonlocal small-scale parameter and geometry of SLGS on its vibrational frequency response. Then, molecular dynamics simulation with some specified defects is performed and the obtained frequency response is compared with nonlocal continuum results to calibrate a proper value for the nonlocal small scale parameter finding a good agreement.

2. Nonlocal continuum elasticity for defective SLGSs

In the continuum mechanics approach, let us consider a rectangular nanoplate of length a, width b, effective thickness h and mass density ρ with an initial geometric imperfection, w^*, (Fig. 1). It is assumed that the initial geometric imperfection exists only along transverse direction and the imperfect nanoplate is in a stress-free situation. It has been proved [39] that neglecting shear deformations of a plate with large thickness to length size ratio significantly decreases the validity of plate model in comparison with the exact elasticity solution. In order to improve the accuracy of the results, the first order shear

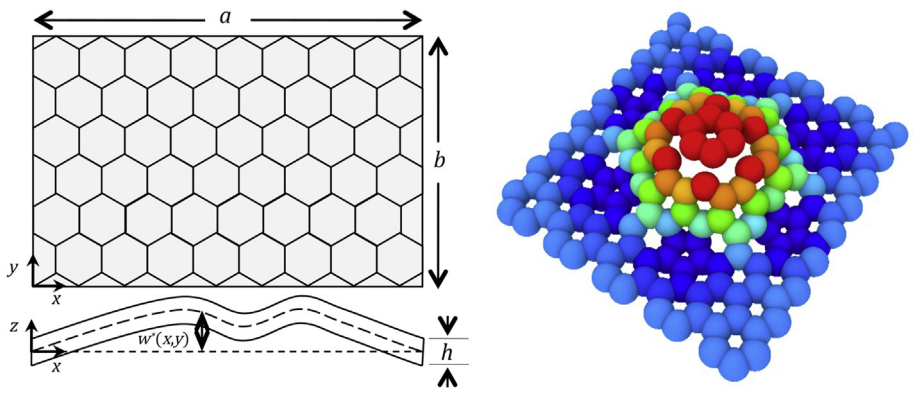

Fig. 1. Continuum and molecular models of out-of-plane defective SLGSs.

deformation plate theory (FSDT), which considers shear deformations, is implemented to define displacements field as follows:

$$U(x,y,z,t) = u_0(x,y,t) + z\varphi_x(x,y,t) \tag{1a}$$

$$V(x,y,z,t) = v_0(x,y,t) + z\varphi_y(x,y,t) \tag{1b}$$

$$W(x,y,z,t) = w_0(x,y,t) + w^*(x,y) \tag{1c}$$

The five shown independent variables u_0, v_0, w_0, φ_x, and φ_y are the mid-plane displacement components along the x, y and z directions and rotations about y-axis, and x-axis, respectively, and t defines time. The strain–displacement relations for small deformations are defined as:

$$\varepsilon_x = u_{0,x} + w_{0,x}w^*_{,x} + z\varphi_{x,x} \tag{2a}$$

$$\varepsilon_y = v_{0,y} + w_{0,y}w^*_{,y} + z\varphi_{y,y} \tag{2b}$$

$$\gamma_{xy} = u_{0,y} + v_{0,x} + w_{0,x}w^*_{,y} + w_{0,y}w^*_{,x} + z\left(\varphi_{x,y} + \varphi_{y,x}\right) \tag{2c}$$

$$\gamma_{xz} = \varphi_x + w_{0,x} \tag{2d}$$

$$\gamma_{zy} = \varphi_y + w_{0,y} \tag{2e}$$

where $(\,)_{,\boldsymbol{x}}$ and $(\,)_{,\boldsymbol{y}}$ indicate the differentiation with respect to x and y, respectively. To consider discrete nature of SLGSs, size effect could be adopted to the continuum formulation by introducing the nonlocal small scale parameter, $\boldsymbol{\mu} = (\boldsymbol{e_0 a_0})^2$. ($e_0$ is a material constant, a_0 is the internal characteristic length) [35], and modifying constitutive stress–strain relations. For brevity, we ignored explaining step-by-step details for adding nonlocal effects to equations of motion. However, an extensive review on employing the nonlocal elasticity for modeling carbon nanotubes and graphene could be found in Ref. [36]. By employing the Hamilton's principle, the nonlocal governing equations of motion can be obtained as [39]:

$$\begin{aligned} A\Big[&\left(u_{0,xx} + w_{0,xx}w^*_{,x} + w_{0,x}w^*_{,xx}\right) + v\left(v_{0,xy} + w_{0,xy}w^*_{,y} + w_{0,y}w^*_{,xy}\right) + \frac{(1-v)}{2}\left(u_{0,yy} + v_{0,xy} + w_{0,xy}w^*_{,y} + w_{0,x}w^*_{,yy}\right. \\ &\left. + w_{0,yy}w^*_{,x} + w_{0,y}w^*_{,xy}\right)\Big] \\ &= I_0\left(\ddot{u}_0 - \mu\ddot{u}_{0,xx} - \mu\ddot{u}_{0,yy}\right) \end{aligned} \tag{3a}$$

$$\begin{aligned} A\Big[&v\left(u_{0,xy} + w_{0,xy}w^*_{,x} + w_{0,x}w^*_{,xy}\right) + \left(v_{0,yy} + w_{0,yy}w^*_{,y} + w_{0,y}w^*_{,yy}\right) + \frac{(1-v)}{2}\left(v_{0,xx} + u_{0,xy} + w_{0,xx}w^*_{,y} + w_{0,x}w^*_{,xy}\right. \\ &\left. + w_{0,xy}w^*_{,x} + w_{0,y}w^*_{,xx}\right)\Big] \\ &= I_0\left(\ddot{v}_0 - \mu\ddot{v}_{0,xx} - \mu\ddot{v}_{0,yy}\right) \end{aligned} \tag{3b}$$

$$A\left[K_s\frac{(1-\nu)}{2}\left(w_{0,xx}+w_{0,yy}+\varphi_{x,x}+\varphi_{y,y}\right)+w^*_{,xx}\left[\left(u_{0,x}+w_{0,x}w^*_{,x}\right)+\nu\left(v_{0,y}+w_{0,y}w^*_{,y}\right)\right]+w^*_{,yy}\left[\left(v_{0,y}+w_{0,y}w^*_{,y}\right)\right.\right.$$
$$\left.\left.+\nu\left(u_{0,x}+w_{0,x}w^*_{,x}\right)\right]+(1-\nu)w^*_{,xy}\left(u_{0,y}+v_{0,x}+w_{0,x}w^*_{,y}+w_{0,y}w^*_{,x}\right)\right] \tag{3c}$$
$$=I_0\left(\ddot{w}_0-\mu\ddot{w}_{0,xx}-\mu\ddot{w}_{0,yy}\right)$$

$$D\left[\varphi_{x,xx}+\nu\varphi_{y,xy}+\frac{1-\nu}{2}\left(\varphi_{x,yy}+\varphi_{y,xy}\right)\right]-K_sA\frac{(1-\nu)}{2}\left(\varphi_x+w_{0,x}\right)=I_2\left(\ddot{\varphi}_x-\mu\ddot{\varphi}_{x,xx}-\mu\ddot{\varphi}_{x,yy}\right) \tag{3d}$$

$$D\left[\varphi_{y,yy}+\nu\varphi_{x,xy}+\frac{1-\nu}{2}\left(\varphi_{y,xx}+\varphi_{x,xy}\right)\right]-K_sA\frac{(1-\nu)}{2}\left(\varphi_y+w_{0,y}\right)=I_2\left(\ddot{\varphi}_y-\mu\ddot{\varphi}_{y,xx}-\mu\ddot{\varphi}_{y,yy}\right) \tag{3e}$$

where $A=Eh/(1-\nu^2)$ and $D=Eh^3/[12(1-\nu^2)]$ are the longitudinal and flexural rigidity of the nanoplate, respectively (E and ν are Young's modulus and Poison's ratio of the nanoplate) and K_s is the shear correction factor of FSDT set to 5/6 [39]. Also, $(\dot{})$ indicates differentiation with respect to t and I_0 and I_2 are mass moments of inertia which are defined as follows:

$$(I_0,I_2)=\int_{-h/2}^{h/2}\rho\left(1,z^2\right)dz \tag{4}$$

Reviewing the literature reveals that the boundary conditions of SLGSs needs to be explain more clearly. Ref. [40] has reported both clamped and simply supported edges for SLGSs. In the nonlocal continuum model, as a nanoplate, it is possible to consider both boundaries. However, in MD simulations it was suggested to fixed one layer of carbon atoms for mimicking simply supported edges while four layers of carbon atoms needed to be fixed in clamped boundaries with zero slope. This assumption may cause a misunderstanding: From classical structural mechanics, it is known that a plate with clamped boundaries has higher frequency than a simply supported one. One the other hand, it is known that when the length size of a plate reduces, its frequency increases. In MD simulations, when four layers of carbon atoms are fixed, these atoms are not vibrating and in fact they are not included in the active area of vibration. Actually, the SLGS margin has been removed and its length size has been reduced. Hence, its frequency increases because of reducing length size not changing the boundary condition of clamped edges. Besides, in MD simulation results, one can see that the carbon atoms close to the fixed edges easily move in transverse direction and the slope of a vibrating graphene sheet in its boundaries is considerably different from zero and cannot be neglected. In real situation when the boundaries of a SLGS are fixed, many layers (more than four layers) of atoms may be attached to the substrate. However, only the active atoms are considered for determining the effective length. The conclusion is that the ideal clamped edges cannot be achieved in SLGSs. Consequently, because of existence of non-zero slope at the edge, in the continuum nonlocal model the edges of SLGS are considered as simply supported. The conditions of simply supported boundaries are:

$$\begin{aligned}&At\ x=0,a: \quad u_0=v_0=w_0=\varphi_y=\varphi_{x,x}=0\\&At\ y=0,b: \quad u_0=v_0=w_0=\varphi_x=\varphi_{y,y}=0\end{aligned} \tag{5}$$

3. Numerical Continuum

In this section, the partial differential Eq. (3) with the associated boundary conditions (5) will be numerically solved using spectral method [41] in order to determine the frequency response of defective SLGSs. It has been reported that pseudo-spectral method (the collocation version of spectral method) can be accurately applied to non-periodic finite domains such as structural problems [42–44]. The main idea in this method is to approximate the derivative of an unknown function, F, at a collocation point by an equivalent weighted linear sum of the function values at all collocation points. For one-dimensional domains it can be written as follows:

$$F^{(n)}_{,x}(x_i)=\sum_{k=0}^{N}d^{(n)}_{ik}F(x_k)\ \ or\ \ \left\{F^{(n)}_{,x}\right\}_{(N+1)\times1}=\left[D^{(n)}\right]_{(N+1)\times(N+1)}\{F\}_{(N+1)\times1} \tag{6}$$

where $(N+1)$ is the number of collocation points, $F^{(n)}_{,x}(x_i)$ indicates nth differentiation of function F in ith collocation point and $[D^{(n)}]$ is called the nth differentiation matrix, whose components can be found based on Chebyshev basic functions [45]. To extent the method to two-dimensional domains, one can compute the nth partial derivative by use of Kronecker products as follows [45]:

$$\left\{\frac{\partial^{(n)}F}{\partial x^{(n)}}\right\}_{(N+1)^2\times 1} = \left[\boldsymbol{D}^{(n)}\otimes\boldsymbol{I}\right]_{(N+1)^2\times(N+1)^2}\{F\}_{(N+1)^2\times 1}, \tag{7a}$$

$$\left\{\frac{\partial^{(m)}F}{\partial y^{(m)}}\right\}_{(N+1)^2\times 1} = \left[\boldsymbol{I}\otimes\boldsymbol{D}^{(m)}\right]_{(N+1)^2\times(N+1)^2}\{F\}_{(N+1)^2\times 1} \tag{7b}$$

$$\left\{\frac{\partial^{(n+m)}F}{\partial x^{(n)}\partial y^{(m)}}\right\}_{(N+1)^2\times 1} = \left[\boldsymbol{D}^{(n)}\otimes\boldsymbol{I}\right]_{(N+1)^2\times(N+1)^2}\left[\boldsymbol{I}\otimes\boldsymbol{D}^{(m)}\right]_{(N+1)^2\times(N+1)^2}\{F\}_{(N+1)^2\times 1} \tag{7c}$$

The Basic functions (Chebyshev polynomials) are orthogonal in the range of [−1,1] and consequently the differentiation matrix components, $[D^{(n)}]$, are defined in this range. Therefore, the rectangular real domain of nanoplate needs to be mapped to a 2 × 2 square computational domain by the following transformations:

$$\bar{x} = \frac{2x}{a} - 1, \quad \bar{y} = \frac{2y}{b} - 1, \quad \bar{x},\bar{y}\in[-1,1] \tag{8}$$

For the purpose of optimum distribution, the grid points in both $\bar{x}$. and $\bar{y}$ directions are selected based on the Gauss–Lobatto interpolation points as [41].

$$\bar{x}_i = \cos\left(\frac{\pi i}{N}\right), \quad \bar{y}_j = \cos\left(\frac{\pi j}{N}\right), \quad i,j = 0,1,2,\ldots,N \tag{9}$$

Also, the following dimensionless parameters are introduced to make the problem dimensionless:

$$\begin{aligned}&\left(\bar{u}_0,\bar{v}_0,\bar{w}_0,\bar{w}^*\right) = \left(u_0,v_0,w_0,w^*\right)/h, \quad \alpha = h/a, \quad \beta = h/b, \quad \gamma = a/b,\\ &\bar{\mu} = \mu/a^2, \quad \bar{t} = \frac{t}{h}\sqrt{A/I_0}\left(\bar{\omega} = \Omega h\sqrt{I_0/A}\right),\end{aligned} \tag{10}$$

where Ω and $\bar{\omega}$ are the factual and dimensionless natural frequency of the system, respectively. Namely, the dimensionless displacement components are assumed as:

$$\begin{Bmatrix}\bar{u}_0(\bar{x},\bar{y},\bar{t})\\ \bar{v}_0(\bar{x},\bar{y},\bar{t})\\ \bar{w}_0(\bar{x},\bar{y},\bar{t})\\ \varphi_x(\bar{x},\bar{y},\bar{t})\\ \varphi_y(\bar{x},\bar{y},\bar{t})\end{Bmatrix} = \begin{Bmatrix}\bar{u}_0(\bar{x},\bar{y})\\ \bar{v}_0(\bar{x},\bar{y})\\ \bar{w}_0(\bar{x},\bar{y})\\ \varphi_x(\bar{x},\bar{y})\\ \varphi_y(\bar{x},\bar{y})\end{Bmatrix} e^{i\bar{\omega}\bar{t}} \tag{11}$$

Substituting Eqs. (8), (10) and (11) into Eqs. (3) and (5), One can obtain the dimensionless eigenvalue problem for free vibration of defective SLGSs in the following forms:

$$\begin{aligned}&4\alpha^2\bar{u}_{,\bar{x}\bar{x}} + 8\alpha^3\left(\bar{w}^*_{,\bar{x}}\bar{w}_{,\bar{x}\bar{x}} + \bar{w}^*_{,\bar{x}\bar{x}}\bar{w}_{,\bar{x}}\right) + \nu\left[4\alpha\beta\bar{v}_{,\bar{x}\bar{y}} + 8\alpha\beta^2\left(\bar{w}^*_{,\bar{y}}\bar{w}_{,\bar{x}\bar{y}} + \bar{w}^*_{,\bar{x}\bar{y}}\bar{w}_{,\bar{y}}\right)\right] + \frac{(1-\nu)}{2}\left[4\beta^2\bar{u}_{,\bar{y}\bar{y}} + 4\alpha\beta\bar{v}_{,\bar{x}\bar{y}}\right.\\ &\left. + 8\alpha\beta^2\left(\bar{w}^*_{,\bar{y}}\bar{w}_{,\bar{x}\bar{y}} + \bar{w}^*_{,\bar{x}}\bar{w}_{,\bar{y}\bar{y}} + \bar{w}^*_{,\bar{y}\bar{y}}\bar{w}_{,\bar{x}} + \bar{w}^*_{,\bar{x}\bar{y}}\bar{w}_{,\bar{y}}\right)\right]\\ &= -\bar{\omega}^2\left(\bar{u} - 4\bar{\mu}\bar{u}_{,\bar{x}\bar{x}} - 4\gamma^2\bar{\mu}\bar{u}_{,\bar{y}\bar{y}}\right)\end{aligned} \tag{12a}$$

$$\begin{aligned}&4\beta^2\bar{v}_{,\bar{y}\bar{y}} + 8\beta^3\left(\bar{w}^*_{,\bar{y}}\bar{w}_{,\bar{y}\bar{y}} + \bar{w}^*_{,\bar{y}\bar{y}}\bar{w}_{,\bar{y}}\right) + \nu\left[4\alpha\beta\bar{u}_{,\bar{x}\bar{y}} + 8\alpha^2\beta\left(\bar{w}^*_{,\bar{x}}\bar{w}_{,\bar{x}\bar{y}} + \bar{w}^*_{,\bar{x}\bar{y}}\bar{w}_{,\bar{x}}\right)\right] + \frac{(1-\nu)}{2}\left[4\alpha^2\bar{v}_{,\bar{x}\bar{x}} + 4\alpha\beta\bar{u}_{,\bar{x}\bar{y}}\right.\\ &\left. + 8\alpha^2\beta\left(\bar{w}^*_{,\bar{x}}\bar{w}_{,\bar{x}\bar{y}} + \bar{w}^*_{,\bar{y}}\bar{w}_{,\bar{x}\bar{x}} + \bar{w}^*_{,\bar{x}\bar{x}}\bar{w}_{,\bar{y}} + \bar{w}^*_{,\bar{x}\bar{y}}\bar{w}_{,\bar{x}}\right)\right]\\ &= -\bar{\omega}^2\left(\bar{v} - 4\bar{\mu}\bar{v}_{,\bar{x}\bar{x}} - 4\gamma^2\bar{\mu}\bar{v}_{,\bar{y}\bar{y}}\right)\end{aligned} \tag{12b}$$

$$K_s\frac{(1-\nu)}{2}\left[4\alpha^2\overline{w}_{,\overline{x}\overline{x}}+4\beta^2\overline{w}_{,\overline{y}\overline{y}}+2\alpha\overline{\varphi}_{x,\overline{x}}+2\beta\overline{\varphi}_{y,\overline{y}}\right]+4\alpha^2\overline{w}^*_{,\overline{x}\overline{x}}\left[\left(2\alpha\overline{u}_{,\overline{x}}+4\alpha^2\overline{w}^*_{,\overline{x}}\overline{w}_{,\overline{x}}\right)+\nu\left(2\beta\overline{v}_{,\overline{y}}+4\beta^2\overline{w}^*_{,\overline{y}}\overline{w}_{,\overline{y}}\right)\right]+4\beta^2\overline{w}^*_{,\overline{y}\overline{y}}$$
$$\left[\left(2\beta\overline{v}_{,\overline{y}}+4\beta^2\overline{w}^*_{,\overline{y}}\overline{w}_{,\overline{y}}\right)+\nu\left(2\alpha\overline{u}_{,\overline{x}}+4\alpha^2\overline{w}^*_{,\overline{x}}\overline{w}_{,\overline{x}}\right)\right]+4(1-\nu)\alpha\beta\overline{w}^*_{,\overline{x}\overline{y}}\left[2\beta\overline{u}_{,\overline{y}}+2\alpha\overline{v}_{,\overline{x}}+4\alpha\beta\left(\overline{w}^*_{,\overline{x}}\overline{w}_{,\overline{y}}+\overline{w}^*_{,\overline{y}}\overline{w}_{,\overline{x}}\right)\right]$$
$$=-\overline{\omega}^2\left(\overline{w}-4\overline{\mu}\overline{w}_{,\overline{x}\overline{x}}-4\gamma^2\overline{\mu}\overline{w}_{,\overline{y}\overline{y}}\right) \tag{12c}$$

$$4\alpha^2\overline{\varphi}_{x,\overline{x}\overline{x}}+4\nu\alpha\beta\overline{\varphi}_{y,\overline{x}\overline{y}}+2(1-\nu)\left(\beta^2\overline{\varphi}_{x,\overline{y}\overline{y}}+\alpha\beta\overline{\varphi}_{y,\overline{x}\overline{y}}\right)-6K_s(1-\nu)\left(\overline{\varphi}_x+2\alpha\overline{w}_{,\overline{x}}\right)=-\overline{\omega}^2\left(\overline{\varphi}_x-4\overline{\mu}\overline{\varphi}_{x,\overline{x}\overline{x}}-4\gamma^2\overline{\mu}\overline{\varphi}_{x,\overline{y}\overline{y}}\right) \tag{12d}$$

$$4\beta^2\overline{\varphi}_{y,\overline{y}\overline{y}}+4\nu\alpha\beta\overline{\varphi}_{x,\overline{x}\overline{y}}+2(1-\nu)\left(\alpha^2\overline{\varphi}_{y,\overline{x}\overline{x}}+\alpha\beta\overline{\varphi}_{x,\overline{x}\overline{y}}\right)-6K_s(1-\nu)\left(\overline{\varphi}_y+2\beta\overline{w}_{,\overline{y}}\right)=-\overline{\omega}^2\left(\overline{\varphi}_y-4\overline{\mu}\overline{\varphi}_{y,\overline{x}\overline{x}}-4\gamma^2\overline{\mu}\overline{\varphi}_{y,\overline{y}\overline{y}}\right) \tag{12e}$$

and the dimensionless boundary conditions are.

$$\begin{array}{ll}At\ \overline{x}=-1,+1: & \overline{u}=\overline{v}=\overline{w}=\overline{\varphi}_y=\overline{\varphi}_{x,\overline{x}}=0\\ At\ \overline{y}=-1,+1: & \overline{u}=\overline{v}=\overline{w}=\overline{\varphi}_x=\overline{\varphi}_{y,\overline{y}}=0\end{array} \tag{13}$$

The discrete form of the problem based on the pseudo-spectral method can be obtained by applying Eq. (7) to Eqs. (12) and (13), which is written in the following matrix form:

$$\left(\begin{bmatrix}\boldsymbol{k}_{11} & \boldsymbol{k}_{12} & \boldsymbol{k}^*_{13} & 0 & 0\\ \boldsymbol{k}_{21} & \boldsymbol{k}_{22} & \boldsymbol{k}^*_{23} & 0 & 0\\ \boldsymbol{k}^*_{31} & \boldsymbol{k}^*_{32} & \boldsymbol{k}_{33}+\boldsymbol{k}^*_{33} & \boldsymbol{k}_{34} & \boldsymbol{k}_{35}\\ 0 & 0 & \boldsymbol{k}_{43} & \boldsymbol{k}_{44} & \boldsymbol{k}_{45}\\ 0 & 0 & \boldsymbol{k}_{53} & \boldsymbol{k}_{54} & \boldsymbol{k}_{55}\end{bmatrix}+\overline{\omega}^2\begin{bmatrix}\boldsymbol{m}_{11} & 0 & 0 & 0 & 0\\ 0 & \boldsymbol{m}_{22} & 0 & 0 & 0\\ 0 & 0 & \boldsymbol{m}_{33} & 0 & 0\\ 0 & 0 & 0 & \boldsymbol{m}_{44} & 0\\ 0 & 0 & 0 & 0 & \boldsymbol{m}_{55}\end{bmatrix}\right)\begin{Bmatrix}\overline{\boldsymbol{u}}\\ \overline{\boldsymbol{v}}\\ \overline{\boldsymbol{w}}\\ \overline{\boldsymbol{\varphi}}_{\boldsymbol{x}}\\ \overline{\boldsymbol{\varphi}}_{\boldsymbol{y}}\end{Bmatrix}=\{0\} \tag{14}$$

where $\boldsymbol{k}_{ij}$, and $\boldsymbol{m}_{ii}$ are the stiffness and mass components related to a perfect nanoplate and $\boldsymbol{k}^*_{ij}$ matrices contain the effect of the initial geometric imperfection and their description is presented in Appendix A. From Eq. (14), it is seen that the presence of geometric imperfection causes a coupling between in-plane and transverse motions. It can be concluded that the assumed in-plane boundary conditions will also affect transverse vibration frequencies. In order to establish the standard eigenvalue form of the problem, the displacement vectors can be divided into the boundary and the domain parts as follows:

$$\begin{Bmatrix}\overline{\boldsymbol{u}}_{\boldsymbol{b}}\\ \overline{\boldsymbol{v}}_{\boldsymbol{b}}\\ \overline{\boldsymbol{w}}_{\boldsymbol{b}}\\ \overline{\boldsymbol{\varphi}}_{\boldsymbol{xb}}\\ \overline{\boldsymbol{\varphi}}_{\boldsymbol{yb}}\end{Bmatrix}=\{b\},\quad\begin{Bmatrix}\overline{\boldsymbol{u}}_{\boldsymbol{d}}\\ \overline{\boldsymbol{v}}_{\boldsymbol{d}}\\ \overline{\boldsymbol{w}}_{\boldsymbol{d}}\\ \overline{\boldsymbol{\varphi}}_{\boldsymbol{xd}}\\ \overline{\boldsymbol{\varphi}}_{\boldsymbol{yd}}\end{Bmatrix}=\{d\} \tag{15}$$

where the subscripts b and d indicate boundary and domain, respectively. The resulting eigenvalue equations can be written in the matrix form as:

$$\left(\begin{bmatrix}\boldsymbol{K}_{\boldsymbol{bb}} & \boldsymbol{K}_{\boldsymbol{bd}}\\ \boldsymbol{K}_{\boldsymbol{db}} & \boldsymbol{K}_{\boldsymbol{dd}}\end{bmatrix}+\overline{\omega}^2\begin{bmatrix}0 & 0\\ \boldsymbol{M}_{\boldsymbol{db}} & \boldsymbol{M}_{\boldsymbol{dd}}\end{bmatrix}\right)\begin{Bmatrix}b\\ d\end{Bmatrix}=0 \tag{16}$$

Eliminating the boundary displacement vector $\{b\}$ from Eq. (16) yields:

$$\left([K]+\overline{\omega}^2[M]\right)\{d\}=0 \tag{17a}$$

$$[K]=[K_{dd}]-[K_{db}][K_{bb}]^{-1}[K_{bd}], \tag{17b}$$

$$[M]=[M_{dd}]-[M_{db}][K_{bb}]^{-1}[K_{bd}] \tag{17c}$$

where $[M]$ is the total mass matrix and $[K]$ is the total stiffness matrix which contains the effect of initial geometric imperfections.

Table 1
Dimensionless fundamental frequencies of perfect nanoplates. ($\nu = 0.16$).

γ	α	$\overline{\mu}$	Present	Exact [29]
0.5	0.01	0.00	12.3345	12.3352
		0.01	11.6375	11.6382
		0.10	8.2530	8.2534
	0.10	0.00	12.1011	12.1597
		0.01	11.4173	11.4726
		0.10	8.0968	8.1360
1	0.01	0.00	19.7330	19.7346
		0.01	18.0332	18.0347
		0.10	11.4426	11.4436
	0.10	0.00	19.1478	19.2911
		0.01	17.4985	17.6294
		0.10	11.1034	11.1864

4. MD simulations

MD simulation has been carried out by using the open source renowned software i.e. large-scale atomic/molecular massively parallel simulator (LAMMPS) through a velocity-Verlet algorithm with a time step of 0.5 fs to integrate the Newton's equations of motion. Since, the considered system only contains carbon atoms, the adaptive intermolecular reactive empirical bond order potential (AIREBO) [46] is applied. AIREBO potential contains three types of interactions: the famous hydrocarbon REBO potential [47] for modeling short ranged C–C covalent interactions, 4-body torsion potentials, and the standard Lennard–Jones potential.

Simulation is fulfilled following these steps: At the first, the defective SLGS, which is created by manipulating perfect structure of graphene, allowed to be freely relaxed in a desired temperature for a long enough time period by applying the Nose–Hoover thermostat [48] to achieve the stable state of SLGS with the desired out-of-plane defect. Since the present continuum model do not consider thermal effects, for the possibility of comparison, all MD simulations are performed at low temperature conditions, i.e. 1 K. Boundary conditions are implemented by fixing motion of one layer of carbon atoms at the edges of SLGS. It should be mentioned that these boundaries determine the active area of SLGS in vibrating motion and the length and the width of SLGS are specified based on these boundaries. Then, the vibrational motion can be simulated applying an initial velocity, $V_0 = v_{max} sin(\pi x/a) sin(\pi y/b)$, associated to its approximate fundamental mode shape, where v_{max} is the maximum initial velocity at the center of the SLGS. Here, we used $v_{max} = 0.5$ Å/ps to make a vibration motion with small amplitude to be comparable with small deformation assumption in continuum model. In order to avoid the effects of the thermostat on free vibration simulation, a constant total energy ensemble (NVE) is applied and the SLGS is allowed to vibrate freely. The natural frequency is captured from the lateral position trajectory of every moving carbon atom (we used central atom) of the SLGS during a long enough time period (80 fs) by implementing the fast Fourier transform (FFT) method.

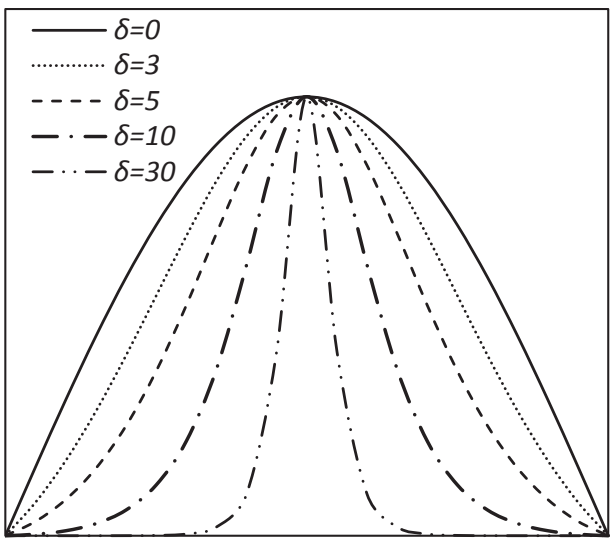

Fig. 2. Controlling the extension of out-of-plane defect on the surface of SLGSs by changing δ parameter.

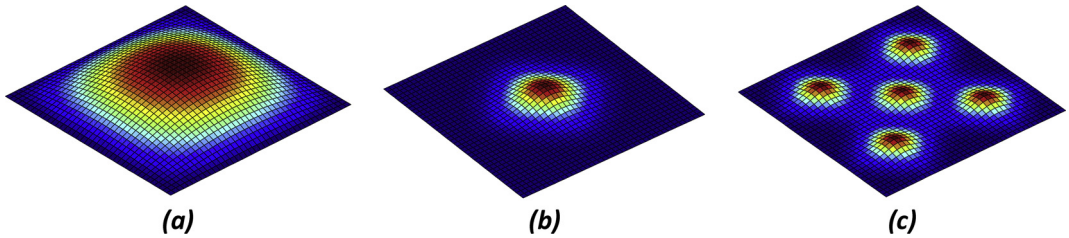

Fig. 3. Three types of out-of-plane defects defined by Eq. (18): (a) sinusoidal defect with $\delta = 0$, $x_c/a = y_c/b = 0.5$, $\xi = 1$. (b) Bulge defect with $\delta = 8$, $x_c/a = y_c/b = 0.5$, $\xi = 0.6$. (c) Five bulge defects dispersed on the surface of the SLGS with $\delta = 12$, $\xi = 0.6$, (x_c/a, y_c/b) equal to (0.25, 0.25), (0.5, 0.5), (0.75, 0.75), (0.25, 75), and (0.75, 0.25).

5. Results and discussion

5.1. Parametric vibration study of defective SLGSs

In this section, the influence of effective parameters i.e., nonlocal small-scale parameter, thickness to side ratio, and amplitude, frequency and location of defects on fundamental frequency response of SLGSs is studied in detail. First of all, in order to verify the accuracy of presented formulations and mathematical model, dimensionless fundamental frequencies of a perfect flat nanoplate ($w^* = 0$) with various thickness to side ratios, α, aspect ratios, γ, and dimensionless nonlocal parameter, $\overline{\mu}$, are listed in Table 1 and compared with the analytical results obtained using nonlocal FSDT plate model [29]. A good agreement is observed confirming the efficiency of the present method. It is seen that increasing size effects ($\overline{\mu}$), increasing thickness to side ratio (α), and decreasing aspect ratio (β), all results in decreasing the dimensionless frequency of the nanoplate.

The initial geometric imperfection, $w^*(x,y)$, which describes the considered defects of SLGSs, is defined as a surface that best fits the shape of the defective SLGS. Although it is possible to consider any arbitrary function as an initial imperfection, for parametric study of amplitude, frequency and location we adopt [49]:

$$w^*(x,y) = \xi h \operatorname{sech}(\delta(x - x_c)/a)\cos(\pi(x - x_c)/a)\operatorname{sech}(\delta(y - y_c)/b)\cos(\pi(y - y_c)/b) \tag{18}$$

where trigonometric cosine functions create a transverse bulge with the maximum located at (x_c, y_c) with amplitude to thickness ratio of ξ and extension controlled by δ parameter. When δ equals to zero, the transverse bulge is fully extended on the surface of the SLGS, while increasing δ concentrates the bulge to the point (x_c, y_c) as it is shown in Fig. 2. The dimensionless initial imperfection is fully described by applying Eqs. (8) and (10) into Eq. (18). Some combination of these parameters and the associated imperfect shapes are presented in Fig. 3.

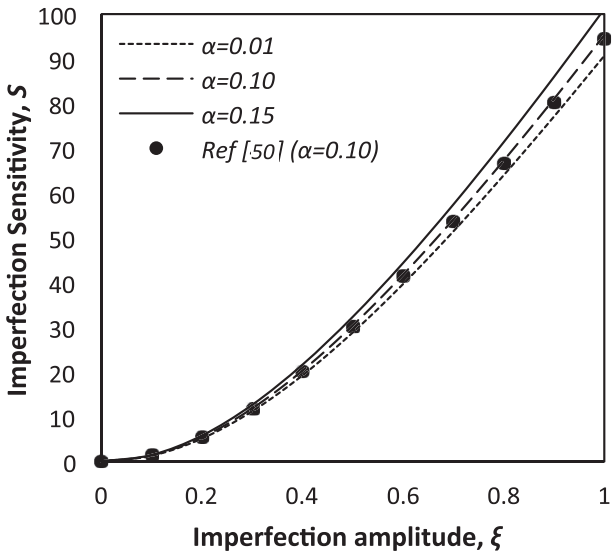

Fig. 4. Influence of dimensionless imperfection amplitude on imperfection sensitivity of SLGSs ($\delta = \mathbf{0}, \mathbf{x_c}/\boldsymbol{a} = \mathbf{y_c}/\boldsymbol{b} = \mathbf{0.5}, \overline{\mu} = \mathbf{0}, \gamma = \mathbf{1}$).

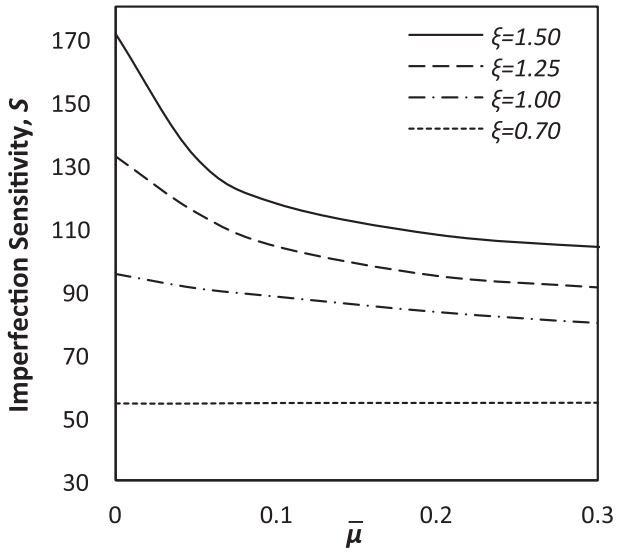

Fig. 5. Influence of dimensionless nonlocal small scale parameter on imperfection sensitivity of SLGSs ($\delta = 0$, $x_c/a = y_c/b = 0.5$, $\alpha = 0.1$, $\gamma = 1$).

To explain quantitatively the influence of initial geometric imperfection on frequency of SLGSs, dimensionless imperfection sensitivity, S, is defined as the percentage of relative changes of fundamental frequency due to presence of initial imperfections, $S = (\overline{\omega}^*/\overline{\omega} - 1) \times 100$, where $\overline{\omega}$ is fundamental frequency of a perfect SLGSs while $\overline{\omega}^*$ is the fundamental frequency of the defective SLGS. Fig. 4 illustrates the variation of imperfection sensitivity, S, versus variation of dimensionless amplitude of defect, ξ, for several values of thickness to side ratios, with ignoring nonlocal effects. The imperfection is considered fully extended and its shape is a sinusoidal surface with one wavelength in every direction ($\delta = 0, x_c/a = y_c/b = 0.5$, $\gamma = 1$). It is seen that increasing the amplitude ξ increases imperfection sensitivity. It means that out-of-plane defects have an enhancing effect on the frequency while SLGSs with larger out-of-plane defects have higher frequency, as it is expected the increasing of the stiffness matrix components. For defect sizes in the order of the thickness ($\xi = 1$), a significant enhancing effect, nearly 100%, is observed, which proves the importance of considering out-of-plane defects on the vibration analysis of SLGS. Also, increasing thickness to side ratio, α, increases the imperfection sensitivity. To validate the present results for defective SLGSs, imperfection sensitivity of macro plates ($\overline{\mu} = 0$) with $\alpha = 0.1$ and sinusoidal imperfection shape reported in [50] are also plotted in Fig. 4 which matches our results nicely.

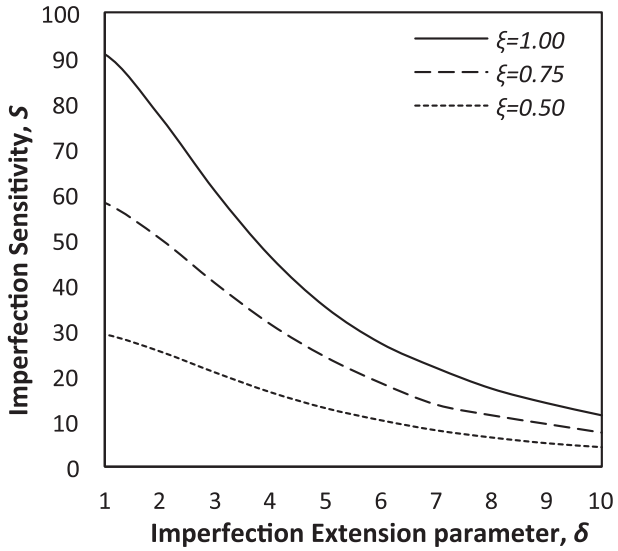

Fig. 6. Influence of Imperfection extension parameter on imperfection sensitivity of SLGSs ($\mathbf{x_c/a = y_c/b = 0.5}, \overline{\mu} = \mathbf{0.1}, \alpha = \mathbf{0.1}, \gamma = \mathbf{1}$.).

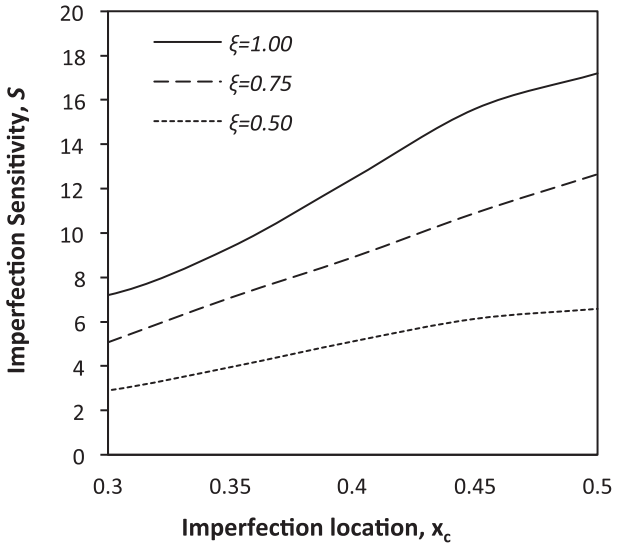

Fig. 7. Influence of Imperfection location on imperfection sensitivity of SLGSs ($\delta = \mathbf{8}, \overline{\mu} = \mathbf{0.1}, \alpha = \mathbf{0.1}, \gamma = \mathbf{1}$.).

Fig. 5 demonstrates the influence of nonlocal size effects on the imperfection sensitivity. The variation of sensitivity is depicted for various values of imperfection amplitude, ξ, with fully extended shape. One can observe that increasing dimensionless nonlocal small scale parameter, $\overline{\mu}$, decreases imperfection sensitivity for every value of ξ. Nevertheless, this decreasing effect is considerable for defects with amplitude in the order of nanoplates thickness or more ($\xi > 1$). For the small scale parameter greater than 0.3 ($\overline{\mu} > 0.3$), the imperfection sensitivity tends to a constant value.

To investigate the influence of extension of out-of-plane defects on the frequency response, the area of SLGSs which is affected by out-of-plane defect, is changed by varying δ parameter and results are depicted for various values of imperfection amplitude, ξ, in Fig. 6. The out-of-plane defect is assumed at the center of square SLGSs. It is seen that increasing δ, which decreases the extension of imperfection and concentrates it at the center of SLGS, results in decreasing imperfection sensitivity. It should be noted that increasing δ to large values (e.g. greater than 20) f a constant ξ results in formation of an ideal sharp high out-of plane defect with small area of extension.

Finally, the effect of defect location on frequency response is investigated. An out-of-plane defect with extension of $\delta = 8$ is assumed to be moved from the point $x_c/a = y_c/b = 0.3$ to the center ($x_c/a = y_c/b = 0.5$). Variation of imperfection sensitivity due

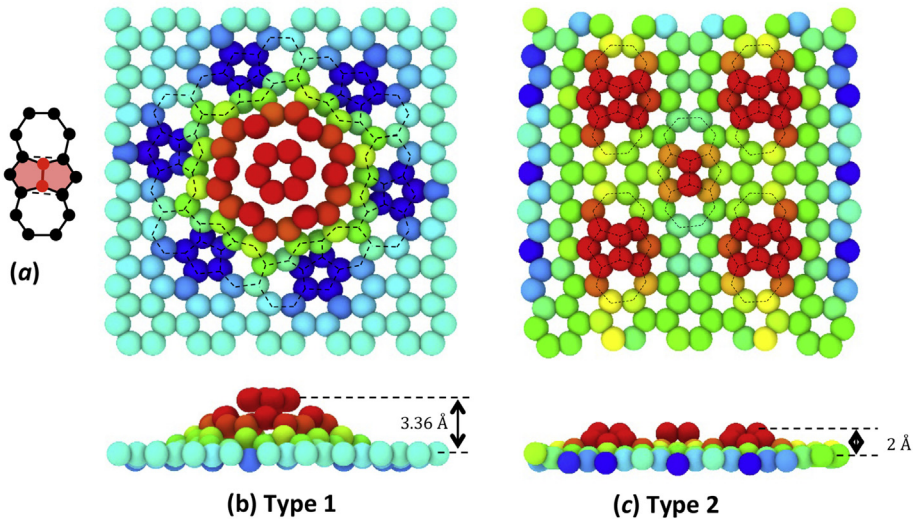

Fig. 8. Two types of stable out-of-plane defects of SLGSs inserting inverse Stone–Wales (ISW) defects in MD simulations: (a) atomic arrangement of an ISW defect. (b) Out-of-plane defect by arranging six ISW defects having the maximum height of 3.36 Å. (c) Out-of-plane defect consisting of an array of five dispersed ISW defects with the maximum height of 2 Å.

Table 2
Comparison between continuum and MD simulations frequencies (GHz) of out-of-plane defected SLGSs.

	MD	e_0a_0 (nm)	
		0	1.08
Perfect flat	584	1510 (157%)[a]	584 (0%)
Defect type 1	740	2068 (179%)	784 (6%)
Defect type 2	809	2113 (161%)	842 (4%)

[a] Errors relative to MD results.

to defect location ($\overline{\mu} = 0.1, \alpha = 0.1, \gamma = 1$) is plotted for several values of ξ in Fig. 7. When the defect is in the center, the maximum value of imperfection sensitivity is achieved. This result agrees with our physical sense in structural plate problems where changing stiffness and mass close to the center of a vibrating plate with fix boundaries has a larger effect on the frequency than making changes in the areas next to its edges which are almost motionless. It should be noted that it is impossible to locate the center point of defect very close to the corner as the defected SLGS should obey the boundary conditions of the edges. Hence, the value of 0.3 for length size is considered as the minimum distance from the corner.

5.2. Comparison between nonlocal elasticity and MD results

MD simulations for vibrational motion of SLGSs with out-of-plane defects are performed. Then, the observed MD frequencies are compared with those obtained by nonlocal continuum elasticity to explore the proper nonlocal small-scale parameter that matches the results. At first, MD simulation is performed for vibration of a flat perfect SLGS of dimensions 2.08 nm × 1.95 nm to investigate the accuracy of the simulation. Fundamental frequency is obtained equals to 584 GHz which is in agreement with the frequency of a square 2 nm × 2 nm SLGS reported in [51] with a difference less than 6%. After ensuring the reliability of MD results, it will be beneficial to compare this frequency with the result obtained from nonlocal model for vibration of a SLGS having the same size to find a proper small-scale parameter that fits MD results. Properties of SLGS are considered equal to values reported in [52] i.e. Young's modulus $E = 1.06$ TPa, Poisson's ratio $\nu = 0.16$, density $\rho = 2250$ kg/m^3, and effective thickness $h = 0.34$ nm. It is seen that small-scale parameter, $e_0a_0 = 1.08$ nm ($\overline{\mu} = 0.29$) can fit MD for the case of flat SLGSs.

Then, MD simulation is performed for defective SLGSs. In order to create out-of-plane defects in SLGSs, inverse Stone–Wales (ISW) defect [53] is implemented. ISW defect is synthesized by inserting two adatoms between two parallel carbon bond of a hexagon. It rearranges four hexagons to two pairs of pentagon/heptagon rings with an out of plane defect 2 Å high. It is noted that regular Stone–Wales defect, having separated pentagon rings, is stable in the plane of GSs. Lusk and Carr [21] showed that six ISW defects can be tactfully aligned to form a larger out-of-plane defect with the height of 3.36 Å. This idea is used to make a higher out-of-plane defect. Fig. 8 illustrates these two types of out-of-plane defects which is inserted in SLGSs as the defects “Type 1” and “Type2”.

These two types of defective SLGSs are considered for MD vibration simulation according to the methods explained in Section 4 and the fundamental frequencies are obtained. To compare these MD results for defective SLGSs with the continuum model, these two types of defects should be approximated by a proper initial geometric imperfection function. The defective SLGS of “Type 1” which represents a large bulge at the center of SLGS can be mimicked defining an initial geometric imperfection with $\xi = 1$, $\delta = 5$, and $x_c/a = y_c/b = 0.5$. Also, the defective SLGS of “Type 2” which represents an array of smaller out-of-plane defects consisting five dispersed ISW defects is mimicked by adding five w^* with $\xi = 0.6$, $\delta = 12$ and corresponding locations on the surface of SLGS. In order to verify the validity of continuum nonlocal model with initial geometric imperfections for vibration analysis of out-of-plane defective SLGSs, the fundamental frequencies of a flat, defective “Type 1” and “Type 2” SLGSs are listed in Table 2 with classical elasticity, nonlocal elasticity and MD simulations. One can observe that classical continuum model overestimates frequencies up to 180% and therefore its result is not reliable for such small defective SLGSs. However, the frequencies obtained based on the nonlocal model are close to those observed in MD simulations, which means that the presented continuum model can accurately predict the stiffening effects of out-of-plane defects on frequency of SLGSs. This enhancing effect can be implemented to tune the frequency characteristics of SLGSs by controlling the type, extension, and location of these defects.

6. Conclusion

In the present study, the influence of defects on vibrational behavior of SLGSs is investigated via both nonlocal continuum elasticity and MD simulations. In the continuum model, the SLGS is considered as a nanoplate and out-of-plane defects are inserted into equations of motion as an initial geometric imperfection. The conclusions are listed as follows.

- It is observed in both nonlocal continuum and MD simulation results that out-of-plane defects have an increasing effect on fundamental frequency of SLGSs. Increasing amplitude of defect as well as increasing its extension on the surface of SLGSs both increase the frequency.
- For the specified amplitude and extension of out-of-plane defect, the maximum value of imperfection sensitivity is achieved when the out-of-plane defect is in the center of SLGS and it decreases approaching the edges.
- Classical plate model, which neglects nonlocality, overestimates the frequencies of defected SLGSs with notable errors, while nonlocal plate model can fit MD results by implementing a proper small scale parameter. It is seen that the calibrated small scale parameter obtained by comparison between nonlocal and MD frequencies of flat SLGSs, can also fit continuum and MD frequencies of out-of-plane defected SLGSs with an acceptable accuracy.

Acknowledgments

The financial support of Iran Nanotechnology Initiative Council is gratefully acknowledged.

NMP is supported by the European Research Council (ERC StG Ideas 2011 BIHSNAM no. 279985 on “Bio-Inspired hierarchical super-nanomaterials”, ERC PoC 2015- SILKENE no. 693670 on “Bionic silk with graphene or other nanomaterials spun by silk-worms”, ERC PoC 2013-2 KNOTOUGH no. 632277 on “Super-tough knotted fibres”), by the European Commission under the Graphene Flagship (WP10 “Nanocomposites”, no. 604391) and by the Provincia Autonoma di Trento (“Graphene Nanocomposites”, no. S116/2012-242637 and reg. delib. no. 2266).

Appendix

$$
\begin{aligned}
\boldsymbol{k}_{11} &= 4\alpha^2\left(\boldsymbol{D}^{(2)}\otimes\boldsymbol{I}\right)+2(1-\nu)\beta^2\left(\boldsymbol{I}\otimes\boldsymbol{D}^{(2)}\right)\\
\boldsymbol{k}_{12} &= 2\alpha\beta(1+\nu)\left(\boldsymbol{D}^{(1)}\otimes\boldsymbol{I}\right)\left(\boldsymbol{I}\otimes\boldsymbol{D}^{(1)}\right),\\
\boldsymbol{k}^{*}_{13} &= 8\alpha^3\overline{w}^{*}_{,\bar{x}}\left(\boldsymbol{D}^{(2)}\otimes\boldsymbol{I}\right)+4\alpha\beta^2(1-\nu)\overline{w}^{*}_{,\bar{x}}\left(\boldsymbol{I}\otimes\boldsymbol{D}^{(2)}\right)+4\alpha\beta^2(1+\nu)\overline{w}^{*}_{,\bar{y}}\left(\boldsymbol{D}^{(1)}\otimes\boldsymbol{I}\right)\left(\boldsymbol{I}\otimes\boldsymbol{D}^{(1)}\right)\\
&\quad+\left(8\alpha^3\overline{w}^{*}_{,\bar{x}\bar{x}}+4\alpha\beta^2(1-\nu)\overline{w}^{*}_{,\bar{y}\bar{y}}\right)\left(\boldsymbol{D}^{(1)}\otimes\boldsymbol{I}\right)+4\alpha\beta^2(1+\nu)\overline{w}^{*}_{,\bar{x}\bar{y}}\left(\boldsymbol{I}\otimes\boldsymbol{D}^{(1)}\right),\\
\boldsymbol{k}_{21} &= 2\alpha\beta(1+\nu)\left(\boldsymbol{D}^{(1)}\otimes\boldsymbol{I}\right)\left(\boldsymbol{I}\otimes\boldsymbol{D}^{(1)}\right),\\
\boldsymbol{k}_{22} &= 4\beta^2\left(\boldsymbol{I}\otimes\boldsymbol{D}^{(2)}\right)+2(1-\nu)\alpha^2\left(\boldsymbol{D}^{(2)}\otimes\boldsymbol{I}\right),\\
\boldsymbol{k}^{*}_{13} &= 8\beta^3\overline{w}^{*}_{,\bar{y}}\left(\boldsymbol{I}\otimes\boldsymbol{D}^{(2)}\right)+4\alpha^2\beta(1-\nu)\overline{w}^{*}_{,\bar{y}}\left(\boldsymbol{D}^{(2)}\otimes\boldsymbol{I}\right)+4\alpha^2\beta(1+\nu)\overline{w}^{*}_{,\bar{x}}\left(\boldsymbol{D}^{(1)}\otimes\boldsymbol{I}\right)\left(\boldsymbol{I}\otimes\boldsymbol{D}^{(1)}\right)\\
&\quad+\left(8\beta^3\overline{w}^{*}_{,\bar{y}\bar{y}}+4\alpha^2\beta(1-\nu)\overline{w}^{*}_{,\bar{x}\bar{x}}\right)\left(\boldsymbol{I}\otimes\boldsymbol{D}^{(1)}\right)+4\alpha^2\beta(1+\nu)\overline{w}^{*}_{,\bar{x}\bar{y}}\left(\boldsymbol{D}^{(1)}\otimes\boldsymbol{I}\right),\\
\boldsymbol{k}^{*}_{\boldsymbol{31}} &= \left(8\alpha^3\overline{w}^{*}_{,\bar{x}\bar{x}}+8\alpha\beta^2\nu\overline{w}^{*}_{,\bar{y}\bar{y}}\right)\left(\boldsymbol{D}^{(1)}\otimes\boldsymbol{I}\right)+8(1-\nu)\alpha\beta^2\overline{w}^{*}_{,\bar{x}\bar{y}}\left(\boldsymbol{I}\otimes\boldsymbol{D}^{(1)}\right),\\
\boldsymbol{k}^{*}_{32} &= \left(8\alpha^2\beta\nu\overline{w}^{*}_{,\bar{x}\bar{x}}+8\beta^3\overline{w}^{*}_{,\bar{y}\bar{y}}\right)\left(\boldsymbol{I}\otimes\boldsymbol{D}^{(1)}\right)++8(1-\nu)\alpha^2\beta\overline{w}^{*}_{,\bar{x}\bar{y}}\left(\boldsymbol{D}^{(1)}\otimes\boldsymbol{I}\right),\\
\boldsymbol{k}^{*}_{33} &= 16\left(\alpha^4\overline{w}^{*}_{,\bar{x}}\overline{w}^{*}_{,\bar{x}\bar{x}}+\alpha^2\beta^2\nu\overline{w}^{*}_{,\bar{x}}\overline{w}^{*}_{,\bar{y}\bar{y}}+(1-\nu)\alpha^2\beta^2\overline{w}^{*}_{,\bar{y}}\overline{w}^{*}_{,\bar{x}\bar{y}}\right)\left(\boldsymbol{D}^{(1)}\otimes\boldsymbol{I}\right)+16\left(\beta^4\overline{w}^{*}_{,\bar{y}}\overline{w}^{*}_{,\bar{y}\bar{y}}+\alpha^2\beta^2\nu\overline{w}^{*}_{,\bar{y}}\overline{w}^{*}_{,\bar{x}\bar{x}}\right.\\
&\quad\left.+(1-\nu)\alpha^2\beta^2\overline{w}^{*}_{,\bar{x}}\overline{w}^{*}_{,\bar{x}\bar{y}}\right)\left(\boldsymbol{I}\otimes\boldsymbol{D}^{(1)}\right),\\
\boldsymbol{k}_{33} &= 2K_s(1-\nu)\left[\alpha^2\left(\boldsymbol{D}^{(2)}\otimes\boldsymbol{I}\right)+\beta^2\left(\boldsymbol{I}\otimes\boldsymbol{D}^{(2)}\right)\right],\\
\boldsymbol{k}_{34} &= K_s(1-\nu)\alpha\left(\boldsymbol{D}^{(1)}\otimes\boldsymbol{I}\right),\\
\boldsymbol{k}_{35} &= K_s(1-\nu)\beta\left(\boldsymbol{I}\otimes\boldsymbol{D}^{(1)}\right),\\
\boldsymbol{k}_{43} &= -12K_s\alpha(1-\nu)\left(\boldsymbol{D}^{(1)}\otimes\boldsymbol{I}\right),\\
\boldsymbol{k}_{44} &= 4\alpha^2\left(\boldsymbol{D}^{(2)}\otimes\boldsymbol{I}\right)+2(1-\nu)\beta^2\left(\boldsymbol{I}\otimes\boldsymbol{D}^{(2)}\right)-6K_s(1-\nu)(\boldsymbol{I}\otimes\boldsymbol{I}),\\
\boldsymbol{k}_{45} &= 2\alpha\beta(1+\nu)\left(\boldsymbol{D}^{(1)}\otimes\boldsymbol{I}\right)\left(\boldsymbol{I}\otimes\boldsymbol{D}^{(1)}\right),\\
\boldsymbol{k}_{53} &= -12K_s\beta(1-\nu)\left(\boldsymbol{I}\otimes\boldsymbol{D}^{(1)}\right),\\
\boldsymbol{k}_{54} &= 2\alpha\beta(1+\nu)\left(\boldsymbol{D}^{(1)}\otimes\boldsymbol{I}\right)\left(\boldsymbol{I}\otimes\boldsymbol{D}^{(1)}\right),\\
\boldsymbol{k}_{55} &= 4\beta^2\left(\boldsymbol{I}\otimes\boldsymbol{D}^{(2)}\right)+2(1-\nu)\alpha^2\left(\boldsymbol{D}^{(2)}\otimes\boldsymbol{I}\right)-6Ks(1-\nu)(\boldsymbol{I}\otimes\boldsymbol{I}),\\
m_{ii} &= \boldsymbol{I}-4\overline{\mu}\left(\boldsymbol{D}^{(2)}\otimes\boldsymbol{I}\right)-4\gamma^2\overline{\mu}\left(\boldsymbol{I}\otimes\boldsymbol{D}^{(2)}\right),\quad i=1,\ldots,5
\end{aligned}
\tag{21a}
$$

References

[1] A.K. Geim, K.S. Novoselov, The rise of graphene, Nat. Mater. 6 (2007) 183–191.
[2] E. Keith, J.R. Whitener, Paul E. Sheehan, Graphene synthesis, Diam. Relat. Mater. 46 (2014) 25–34.
[3] Chowdhury Sh, R. Balasubramanian, Recent advances in the use of graphene-family nanoadsorbents for removal of toxic pollutants from wastewater, Adv. Colloid Interfaces (2014) 2035–2056.
[4] C. Soldano, A. Mahmood, E. Dujardin, Production, properties and potential of graphene, Carbon 48 (8) (2010) 2127–2150.
[5] T. Zhang, Q. Xue, Sh Zhang, Dong Mingdong, Theoretical approaches to graphene and graphene-based materials, Nanotoday 7 (3) (2012) 180–200.
[6] A. Hashimoto, K. Suenaga, A. Gloter, K. Urita, S. Iijima, Direct evidence for atomic defects in graphene layers, Nature 430 (7002) (2004) 870–873.
[7] M.P. Ariza, M. Ortiz, Discrete dislocations in graphene, J. Mech. Phys. Solids 58 (2010) 710–734.
[8] J. Zang, S. Ryu, N.M. Pugno, Q. Wang, Q. Tu, M.J. Buehler, X. Zhao, Multifunctionality and control of the crumpling and unfolding of large-area graphene, Nat. Mater (2013), http://dx.doi.org/10.1038/NMAT3542.
[9] B. Mortazavi, S. Ahzi, Thermal conductivity and tensile response of defective graphene: a molecular dynamics study, Carbon 63 (2013) 460–470.
[10] R. Ansari, S. Ajori, B. Motevalli, Mechanical properties of defective single-layered graphene sheets via molecular dynamics simulation, Superlattice Microstruct. 51 (2) (2012) 274–289.
[11] O. Lehtinen, S. Kurasch, A.V. Krasheninnikov, U. Kaiser, Atomic scale study of the life cycle of a dislocation in graphene from birth to annihilation, Nat. Commun. 4 (2013) 2098, http://dx.doi.org/10.1038/ncomms3098.
[12] A. Hexemer, V. Vitelli, E.J. Kramer, G.H. Fredrickson, Monte Carlo study of crystalline order and defects on weakly curved surfaces, Phys. Rev. E 76 (2007) 051604.
[13] T.H. Liu, C.W. Pao, Ch Chang, Effects of dislocation densities and distributions on graphene grain boundary failure strengths from atomistic simulations, Carbon 50 (2012) 3465–3472.
[14] T.H. Liu, G. Gajewski, C.W. Pao, Ch Chang, Structure, energy, and structural transformations of graphene grain boundaries from atomistic simulations, Carbon 49 (2011) 2306–2317.
[15] O.V. Yazyev, S.G. Louie, Topological defects in graphene: dislocations and grain boundaries, Phys. Rev. B 81 (2010) 195420.
[16] A.W. Robertson, C.S. Allen, Y.A. Wu, K. He, J. Olivier, J. Neethling, A.I. Kirkland, J.H. Warner, Spatial control of defect creation in graphene at the nanoscale, Nat. Commun. (2012), http://dx.doi.org/10.1038/ncomms2141.
[17] M. Berthe, S. Yoshida, Y. Ebine, K. Kanazawa, A. Okada, A. Taninaka, et al., Reversible defect engineering of single-walled carbon nanotubes using scanning tunneling microscopy, Nano Lett. 7 (12) (2007) 3623–3627.
[18] Y. Sugimoto, M. Abe, S. Hirayama, N. Oyabu, O. Custance, S. Morita, Atom inlays performed at room temperature using atomic force microscopy, Nat. Mater. 4 (2005) 156–159.
[19] A.V. Krasheninnikov, K. Nordlund, J. Keinonen, Production of defects in supported carbon nanotubes under ion irradiation, Phys. Rev. B 65 (16) (2002), 165423–1–8.
[20] B.W. Smith, D.E. Luzzi, Electron irradiation effects in single wall carbon nanotubes, J. Appl. Phys. 90 (7) (2001) 3509–3515.
[21] M.T. Lusk, L.D. Carr, Creation of graphene allotropes using patterned defects, Carbon 47 (2009) 2226–2232.
[22] M.T. Lusk, L.D. Carr, Nanoengineering defect structures on graphene, Phys. Rev. Lett. 100 (2008) 175503.
[23] T. Zhang, X. Li, H. Gao, Defects controlled wrinkling and topological design in graphene, J. Mech. Phys. Solids 67 (2014) 2–13.
[24] E. Jomehzadeh, M.K. Afshar, C. Galiotis, X. Shi, N.M. Pugno, Nonlinear softening and hardening nonlocal bending stiffness of an initially curved monolayer graphene, Int. J. Non-linear Mech. 56 (2013) 123–131.
[25] Q. Wang, B. Arash, A review on applications of carbon nanotubes and graphenes as nano-resonator sensors, Comp. Mater. Sci. 82 (2014) 350–360.
[26] S.K. Jalali, M.H. Naei, N.M. Pugno, A mixed approach for studying size effects and connecting interactions of planar nano structures as resonant mass sensors, Microsyst. Technol. (2014), http://dx.doi.org/10.1007/s00542-014-2362-x.
[27] T.J. Prasanna Kumar, S. Narendar, S. Gopalakrishnan, Thermal vibration analysis of monolayer graphene embedded in elastic medium based on nonlocal continuum mechanics, Compos. Struct. 100 (2013) 332–342.
[28] E. Jomehzadeh, A.R. Saidi, A study on large amplitude vibration of multilayered graphene sheets, Comput. Mater. Sci. 50 (2011) 1043–1051.
[29] S.C. Pradhan, A. Kumar, Vibration analysis of orthotropic graphene sheets using nonlocal elasticity theory and differential quadrature method, Compos. Struct. 93 (2) (2011) 774–779.
[30] Y. Zhang, L.W. Zhang, K.M. Liew, J.L. Yu, Nonlocal continuum model for large deformation analysis of SLGSs using the kp-Ritz element-free method, Int. J. Non-Linear Mech. 79 (2016) 1–9.
[31] Y. Zhang, L.W. Zhang, K.M. Liew, J.L. Yu, Transient analysis of single-layered graphene sheet using the kp-Ritz method and nonlocal elasticity theory, Appl. Math. Comput. 258 (2015) 489–501.
[32] Y. Zhang, Z.X. Lei, L.W. Zhang, K.M. Liew, J.L. Yu, Nonlocal continuum model for vibration of single-layered graphene sheets based on the element-free kp-Ritz method, Eng. Anal. Bound Elem. 56 (2015) 90–97.
[33] H.S. Shen, Y.M. Xu, C.L. Zhang, Prediction of nonlinear vibration of bilayer graphene sheets in thermal environments via molecular dynamics simulations and nonlocal elasticity, Comput. Methods Appl. Mech. Eng. 267 (2013) 458–470.
[34] B. Arash, Q. Wang, W.H. Duan, Detection of gas atoms via vibration of graphenes, Phys. Lett. A 375 (2011) 2411–2415.
[35] A.C. Eringen, Nonlocal Continuum Field Theories, Springer-Verlag, New York, 2002.
[36] B. Arash, Q. Wang, A review on the application of nonlocal elastic models in modeling of carbon nanotubes and graphenes, Comput. Mater. Sci. 51 (2012) 303–313.
[37] M. Rafiee, X.Q. He, K.M. Liew, Non-linear dynamic stability of piezoelectric functionally graded carbon nanotube-reinforced composite plates with initial geometric imperfection, Int. J. Non-linear Mech. 59 (2014) 37–51.
[38] J. Girish, L.S. Ramachandra, Thermal postbuckled vibrations of symmetrically laminated composite plates with initial geometric imperfections, J. Sound Vib. 282 (3–5) (2005) 1137–1153.
[39] J.N. Reddy, Mechanics of Laminated Composite Plates and Shells: Theory and Analysis, second ed., CRC Press, New York, 2003.
[40] R. Ansari, S. Sahmani, B. Arsh, Nonlocal plate model for free vibrations of single-layered graphene sheets, Phys. Lett. A 375 (1) (2010) 53–62.
[41] J.P. Boyd, Chebyshev and Fourier Spectral Methods, Dover, New York, 2000.
[42] S.K. Jalali, M.H. Naei, A. Poorsolhjouy, Thermal stability analysis of circular functionally graded sandwich plates of variable thickness using pseudo-spectral method, Mater. Des. 31 (2010) 4755–4763.
[43] S.K. Jalali, M.H. Naei, A. Poorsolhjouy, Buckling of circular sandwich plates of variable core thickness and FGM face sheets, Int. J. Struct. Stab. Dyn. 11 (2) (2011) 273–295.
[44] S.K. Jalali, M.H. Naei, N.M. Pugno, Graphene-based resonant sensors for detection of ultra-fine nanoparticles: molecular dynamics and nonlocal elasticity investigations, Nano (2014), http://dx.doi.org/10.1142/S1793292015500241.
[45] L.N. Trefethen, Spectral Methods in Matlab, SIAM, Philadelphia, 2000.
[46] S.J. Stuart, A.B. Tutein, J.A. Harrison, A reactive potential for hydrocarbons with intermolecular interactions, J. Chem. Phys. 112 (2000) 6472–6486.
[47] D.W. Brenner, O.A. Shenderova, J.A. Harrison, S.J. Stuart, B. Ni, S.B. Sinnott, A second-generation reactive empirical bond order (REBO) potential energy expression for hydrocarbons, J. Phys. Condens. Matter 14 (2002) 783–802.
[48] W.G. Hoover, Canonical dynamics: equilibrium phase-space distributions, Phys. Rev. A 31 (1985) 1695–1697.
[49] S. Kitipornchai, J. Yang, K.M. Liew, Semi-analytical solution for nonlinear vibration of laminated FGM plates with geometric imperfections, Int. J. Solids Struct. 41 (2004) 2235–2257.
[50] A. Bhimaraddi, Large amplitude vibrations of imperfect antisymmetric angle-ply laminated plates, J. Sound Vib. 162 (3) (1993) 457–470.

[51] E. Mahmoudinezhad, R. Ansari, Vibration analysis of circular and square single-layered graphene sheets: an accurate spring mass model, Phys. E 47 (2013) 12–16.
[52] S. Kitipornchai, X.Q. He, K.M. Liew, Continuum model for the vibration of multilayered graphene sheets, Phys. Rev. B 72 (2005) 075443.
[53] M. Nardelli, J.-L. Fattebert, D. Orlikowski, C. Roland, Q. Zhao, J. Bernholc, Mechanical properties, defects and electronic behavior of carbon nanotubes, Carbon 38 (2000) 1703–1711.